Talanta 314 (2027) 130865

Contents lists available at ScienceDirect

Talanta

journal homepage: www.elsevier.com/locate/talanta

Point-of-care detection of C-peptide in diabetes management: a novel electrochemical immunosensor based on magnetic iron-oxide nanoflowers

Cristina Tortolini [a], Francesco Dotta [b], Andrea Giacomo Marrani [c], Francesco Amato [c], Andrea Lenzi [a], Liudmyla Storozhuk [d,e], Nguyen Thi Kim Thanh [d,e], Riccarda Antiochia [a,*]

[a] Department of Experimental Medicine, Sapienza University of Rome, V.le Regina Elena 324, 00166, Rome, Italy
[b] Department of Biomedical Sciences, National Research Council, P.le Aldo Moro 7, 00185, Rome, Italy
[c] Department of Chemistry, Sapienza University of Rome, P.le Aldo Moro 5, 00185, Rome, Italy
[d] Biophysics Group, Department of Physics and Astronomy, University College London, Gower Street, London, WC1E 6BT, UK
[e] UCL Healthcare Biomagnetics and Nanomaterials Laboratories, 21 Albemarle Street, London, W1S 4BS, UK

ARTICLE INFO

Keywords:
C-peptide
Electrochemical immunosensor
Magnetic iron-oxide nanoflowers
Graphite screen-printed electrode
Human serum and urine
Diabetes management

ABSTRACT

A novel electrochemical immunosensor for point-of-care detection of C-peptide based on a graphite screen-printed electrode (GP-SPE) modified with magnetic iron-oxide nanoflowers (IONFs) has been developed for diabetes management.

The surface structure, morphology and electrochemical properties of unmodified and modified electrodes were investigated by scanning electron microscopy (SEM), transmission electron microscopy (TEM), energy-dispersive X-ray spectroscopy analysis (EDX), X-ray photoelectron spectroscopy (XPS), Raman spectroscopy, cyclic voltammetry (CV) and electrochemical impedance spectroscopy (EIS), demonstrating the enhanced electrochemical response of the platform modified with magnetic IONFs compared to iron-oxide nanoparticles (IONPs) and to unmodified electrode.

The resulting IONFs/GP-SPE platform exhibited competitive analytical performances, including a wide dynamic range (0.25-4 nM), a low detection limit (70 pM) and excellent selectivity. Lastly, the biosensor has been successfully tested in human serum and urine samples, demonstrating an optimum agreement with a conventional HPLC-UV method.

1. Introduction

Diabetes is a chronic disease which affects over 100 million patients worldwide. C-peptide (connecting peptide) is a short polypeptide chain composed of 31 amino acids, produced during the synthesis of insulin within pancreatic β cells [1,2]. Initially synthesized as part of the pro-insulin molecule, C-peptide functions as a linker connecting the A and B chains of insulin. During the maturation of insulin secretory granules, proinsulin is cleaved by proteolytic enzymes, resulting in the simultaneous release of insulin and C-peptide into the bloodstream in equimolar amounts [3–5]. While insulin is rapidly extracted by the liver [6], C-peptide exhibits negligible hepatic extraction and is primarily cleared by the kidneys [7,8]. This metabolic difference results in C-peptide having a significantly longer half-life (20-35 min) compared to insulin (3-5 min), and maintaining peripheral plasma concentrations roughly five times higher [9–11]. Consequently, C-peptide has emerged as a reliable and stable biomarker for evaluating endogenous insulin secretion and pancreatic β-cell function [12].

The importance of C-peptide detection in diabetes management is multifaceted, spanning from initial diagnosis to the prediction of long-term complications. One of its primary clinical roles is in the differentiation of diabetes types [13–15]. In Type 1 diabetes (T1D), the autoimmune destruction of β cells leads to absolute insulin deficiency, characterized by very low or undetectable C-peptide levels [16]. Conversely, in Type 2 diabetes (T2D), C-peptide levels may be normal or even elevated due to insulin resistance, though they often decline over time as β-cell function deteriorates [17–19].

Beyond classification, C-peptide detection is critical for guiding therapeutic decisions [20–22]. Patients with C-peptide levels below 0.2 nM generally require insulin regardless of the underlying etiology

This article is part of a special issue entitled: Nano Sensors & Biosensors published in Talanta.

* Corresponding author.
E-mail address: riccarda.antiochia@uniroma1.it (R. Antiochia).

https://doi.org/10.1016/j.talanta.2026.130865
Received 28 April 2026; Received in revised form 15 September 2026; Accepted 27 October 2026
Available online 28 October 2026
0039-9140/© 2026 Published by Elsevier B.V.

[19]. Furthermore, C-peptide levels can predict the efficacy of non-insulin treatments, such as glucagon-like peptide-1 receptor agonists (GLP-1 RAs), which require residual β cell function to be effective [18,23], and the risk of microvascular [24,25] and macrovascular complications [26,27], diabetic retinopathy, nephropathy, and neuropathy [28], as well as severe hypoglycemia [29–31].

Current methods for C-peptide detection, such as Enzyme-Linked Immunosorbent Assay (ELISA) [32], radioimmunoassay (RIA) [33], electrochemiluminescence immunoassays (ECLIA) [34], and liquid chromatography-tandem mass spectrometry (LC-MS/MS) [35,36], present several limitations. They are time-consuming and expensive, requiring lengthy processing cycles and large-scale laboratory equipment. Moreover, despite the availability of a reference system, the problem of non-standardized C-peptide assays remains a critical issue [37]. These challenges have driven the demand for Point-of-Care (POC) testing devices that are also rapid, low-cost, sensitive, and capable of operating in complex biological matrices. (Bio)sensors meet these requirements, as they are user-friendly and capable of fast and accurate detection of health biomarkers [38–46].

In recent years, only a small number of biosensors have been developed for C-peptide detection [47]. Among the optical detection, a FRET biosensor was developed by Heyduk et al. [48] using two antibodies modified with fluorophore-labelled complementary oligonucleotides, achieving a limit of detection (LOD) of approximately 50 pM. Another highly sensitive optical approach based on Surface-Enhanced Raman Spectroscopy (SERS) was realized by Zhang et al. [49]. This biosensor was based on a hierarchical gold nanorod-based probe and achieved a remarkably low LOD of 1.76×10^{-10} nM, enabling the simultaneous detection of insulin and C-peptide in human serum. Electrochemiluminescence (ECL) biosensors were also realized combining electrochemical and optical techniques to enhance sensitivity. Liu and co-workers [50] modified an indium tin oxide (ITO) glass with gold nanoparticles (AuNPs), C-peptide Ab, and luminol, as luminescent reagent, to achieve a LOD of 4.7 nM. Another sensitive ECL sensor employed a 3D DNA walking machine and hybridization chain reaction to amplify the signal, reaching an LOD of 5.6 fM in human serum samples [51]. Additionally, a colorimetric lateral flow POC system has been designed by Rao et al. [52] for rapid field use, in both serum and whole blood, providing results within 15 min with a LOD of 0.017 nM. Based on colorimetric detection, Chen et al. [53] realized the first wearable biosensor for C-peptide detection based on a microneedle array with a negative pressure to extract the interstitial fluid (ISF). The device employs a double-antibody sandwich immunoassay and a novel antibody regeneration strategy, allowing for at least 10 consecutive detections on a single chip with minimal signal attenuation.

The electrochemical biosensor developed by Jalalvand et al. [54] based on a boron-doped diamond electrode modified with multiwalled carbon nanotubes, graphene, and ionic liquids, represents the only example of electrochemical biosensor for C-peptide detection so far. When assisted by advanced chemometric methods, the biosensor achieved a LOD of 4.1 pM.

Nanoflowers (NFs) or hierarchical 3D flower-shaped nanostructures have recently attracted particular attention because of their higher surface-to-volume ratio compared to spherical nanoparticles, together with their low cost and eco-friendly preparation method [55–57].

Iron oxide nanoflowers (IONFs) showed interesting features for biosensing applications as the rapid electron transfer between Fe^{2+} and Fe^{3+} ions makes IONFs excellent electrical conductors even at room temperature [58].

In this work we demonstrate the feasibility of a cheap, fast and simple electrochemical platform based on magnetic iron-oxide nanoflowers for the development of a sensitive and selective label-free immunosensor for POC detection of C-peptide, demonstrating its excellent agreement with a conventional HPLC-UV method, when tested in real human serum and urine samples.

2. Materials and methods

2.1. Reagents

Potassium ferricyanide (III) ($K_3[Fe(CN)_6]$), potassium ferrocyanide (II) ($K_4[Fe(CN)_6]$), potassium chloride (KCl) chitosan (Chit, low-molecular-weight deacetylated chitin), acetic acid, 1-Ethyl-3-(3-dimethylaminopropyl) carbodiimide (EDC), and N-Hydroxysuccinimide (NHS), bovine serum albumin (BSA), Iron (III) acetylacetonate (Fe(acac)$_3$, 99.9%), triethylene glycol (TREG, 99%), tetraethylene glycol (TEG, 99%), ethyl acetate (EtAc, 99.8%), sodium tripolyphosphate (STTP), and poly(acrylic acid) (PAA, M_w = 1800 Da),were obtained from Merck (Milan, Italy). Anti-C peptide antibody (ab14181, 1 mg/mL) and Human C-peptide (ab93903, 100 μg) from Abcam (Cambridge, UK).

Iron oxide nanoparticles (magnetite, IONPs) and iron oxide nanoflowers (IONFs) were synthetized according to the method reported by Storozhuk et al. [59], with minor modifications. Briefly, the nanoflowers were prepared via a modified thermal decomposition method in TREG, using 0.07 M Fe(acac)$_3$ as the iron precursor. PAA was added (66 mM) to the reaction mixture to promote the formation of the characteristic flower-like morphology while stabilizing the nanoparticles. The reaction mixture was heated to 180 °C at a rate of 3 °C min^{-1}, followed by heating to 280 °C at 5 °C min^{-1}, where it was maintained for 30 min under continuous magnetic stirring (500 rpm). After cooling to room temperature, a ligand exchange process with STPP was carried out. The nanoflowers (NFs) were subsequently purified by dialysis to remove unreacted precursors and excess reagents, and finally freeze-dried to obtain the IONF powder.

High-purity deionized water (resistance: 18.2 MΩ cm at 25 °C; TOC < 10 μg L^{-1}) obtained from Millipore (Molsheim, France) was used throughout all experiments.

2.2. Apparatus

Cyclic voltammetry (CV), electrochemical impedance spectroscopy (EIS) and differential pulse voltammetry (DPV) measurements were performed using Autolab Potentiostat/Galvanostat (Autolab PGSTAT204, Metrohm, Herisau, Switzerland) and software Nova 1.1 v2.1.6.The experiments were carried out with a graphite screen-printed electrode (GP-SPE, DRP-110, d = 4 mm, Metrohm Italiana, Oreggio, Italy), consisting of a carbon working electrode, a silver pseudo-reference electrode, and a carbon auxiliary electrode.

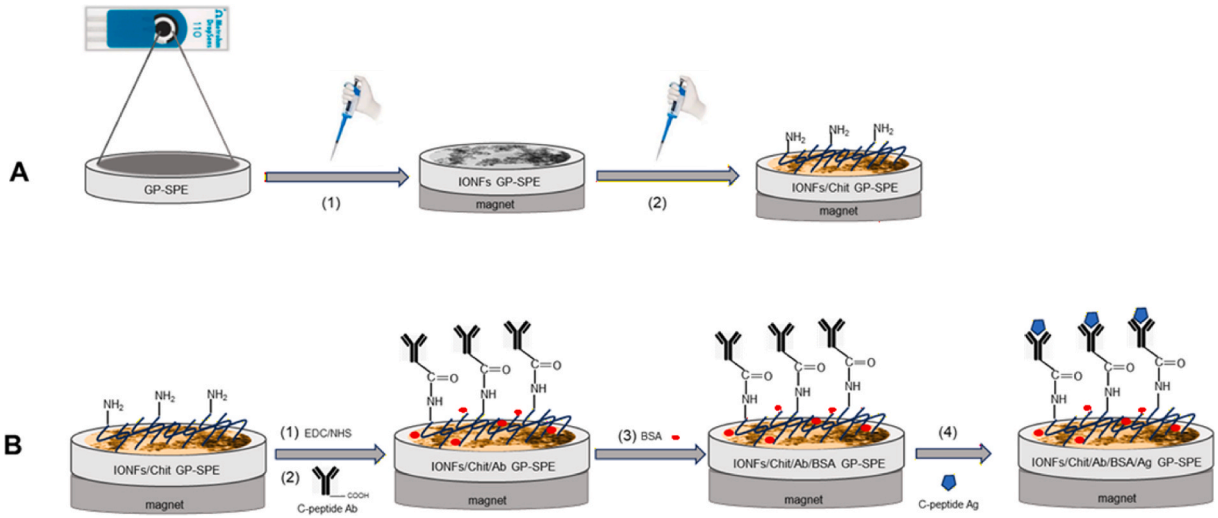
For smartphone-based sensing device experiments, a Sensit Smart portable potentiostat (PalmSens, Houten, Netherlands) was used and directly connected to a smartphone for POC signal reading.

For the study of morphology and composition of the samples, different techniques were used, as follows:

Scanning electron microscopy (SEM) and energy-dispersive X-ray spectroscopy analysis (EDX): SEM and EDX measurements were performed with High-Resolution Field Emission Scanning Electron Microscopy (HR FESEM, Zeiss Auriga Microscopy, Jena, Germany); *Transmission electron microscopy (TEM):* TEM measurements were performed using a JEOL 1200 EX microscope at a 120 kV acceleration voltage. IONFs suspensions (after redispersion in deionized water) were drop-casted on a carbon-coated copper grid and air-dried at room temperature;

Raman spectroscopy: Raman spectra were acquired at room temperature in backscattering geometry with an inVia Renishaw micro-Raman spectrometer equipped with an air-cooled CCD detector and super-Notch filters. An Ar^+ ion laser (λ_{laser} = 514 nm) was used, coupled to a Leica DLML microscope with a 20× objective. The resolution was set to 2 cm^{-1} and the spectra were calibrated using the 520.5 cm^{-1} line of a silicon wafer. Raman spectra were acquired in several (6-10) different spots on the surface of the samples. Each spectrum was acquired with 10% of power, 10 s of spectral acquisition, and 20 scans;

X-ray photoelectron spectroscopy (XPS): the IONFs powder sample was dispersed in distilled water at a concentration of 1 mg mL^{-1} and drop-



Scheme 1. (A) Electrochemical platform and (B) immunosensor fabrication steps.

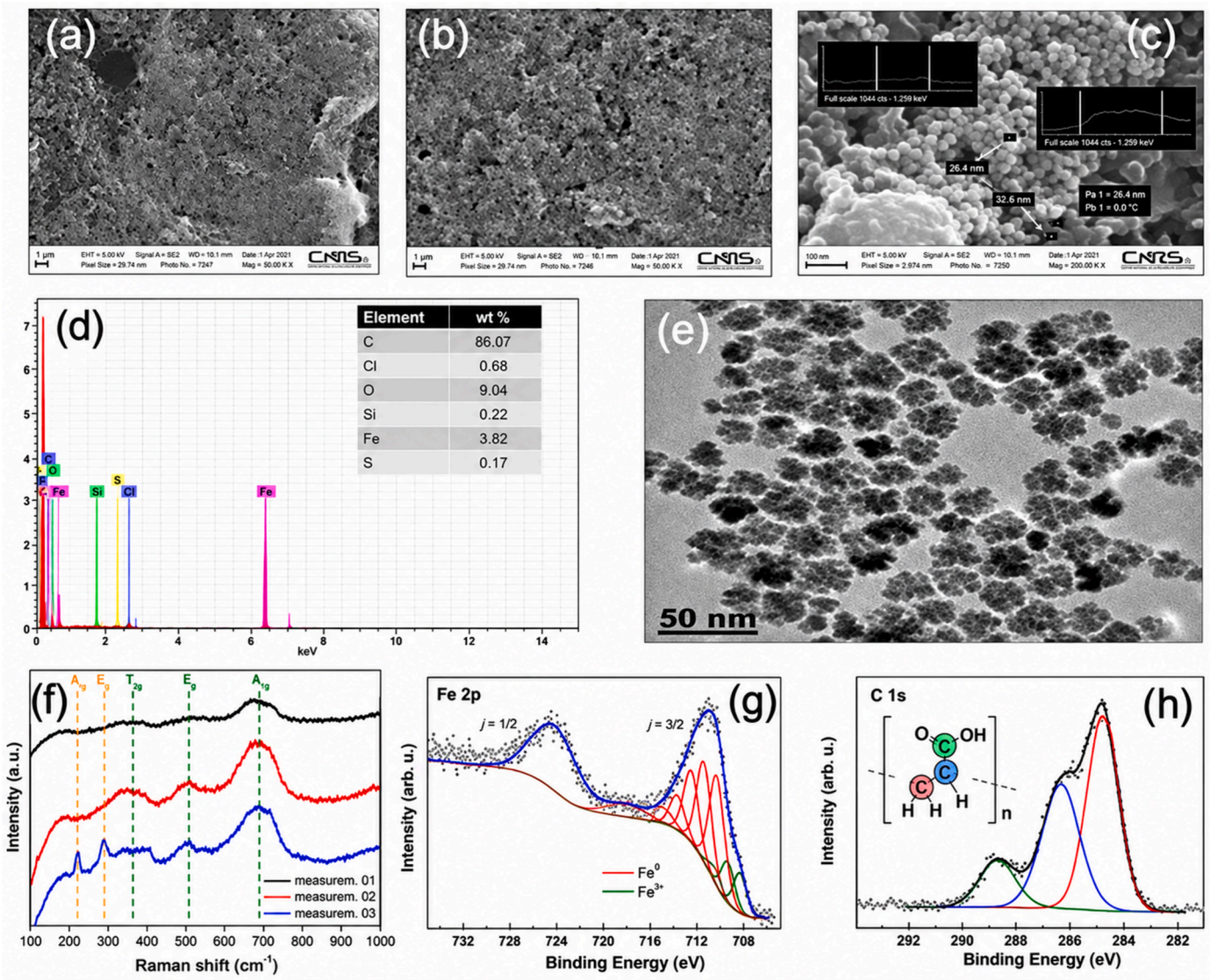


Fig. 1. SEM-EDX spectra of IONFs/GP-SPE at three magnifications: (a) 50.00, (b) 100.00, (c) 300.00 KX; (d) EDX analysis; (e) TEM images of IONFs (scale bar 50 nm); (f) Raman spectra of IONFs recorded on two different spots of the sample; High-resolution XPS spectra of IONFs: (g) Fe 2p region and (h) C 1s region.

casted onto a freshly prepared H-terminated Si(100) wafer and let dry overnight. XPS measurements were carried out using an Omicron NanoTechnology (Uppsala, Sweden) Multiprobe MXPS system equipped with a monochromatic Al Kα (hν = 1486.7 eV) X-ray source (Scienta Omicron XM-1000), applying a 14 kV accelerating voltage and 16 mA emission current. The Fe 2p and C 1s photoionization regions were acquired using an analyzer pass energy of 20 eV. A take-off angle of 21° with respect to the sample surface normal was adopted. The experimental spectra were theoretically reconstructed by fitting the secondary electrons background to a Shirley function and the elastic peaks to pseudo-Voigt functions with a 70:30 Gaussian-Lorentzian ratio.

2.3. Electrochemical measurements

CV, EIS and DPV measurements were conducted in 5 mM $[Fe(CN)_6]^{3-/4-}$ (1:1) solution containing 0.1 M KCl (Zobell's solution). CV curves were recorded in the potential range from − 0.4 to 0.7 V vs. Ag/AgCl at different scan rates. EIS experiments were carried out with a voltage frequency range from 0.1 to 10^5 Hz at amplitude of 5 mV. Parameters in the DPV measurements were as follows: the potential range was from − 0.4 to 0.7 V vs. Ag/AgCl at 0.01 V/s scan rate, a 0.005 V E_{step}, the modulation amplitude was 50 mV, and the modulation time was 0.02 s.

2.4. Immunosensor preparation

2.4.1. Modification steps of electrode surface

The developed electrode was modified by the two following procedures.

- *IONFs/Chit*: 10 μL of a IONFs solution (1 mg/mL in H_2O) was drop-cast on the surface of GP-SPE and let dry at room temperature (RT). Subsequently, 10 μL of 2% Chitosan (in 1% acetic acid solution) was drop-casted on the working surface electrode and let dry at RT. All these steps were applied also by using a magnet, as reported in Scheme 1A (steps 1 and 2);
- *IONPs/Chit*: the same procedure of IONFs/Chit was followed using a IONPs solution.

2.4.2. Electrode surface functionalization

A direct adsorption of the C-peptide antibody (C-peptide Ab) onto the amino-functionalized surface was performed by using the EDC/NHS coupling chemistry. The C-peptide Ab was attached via covalent bonds between its carboxylic group and the amino groups of chitosan.

The immobilization of the C-peptide Ab was realized as follows:

i) drop-casting a mixture of 5 μL of EDC solution (0.5 mM in PBS 0.1 M, pH 7.2, KCl 0.1 M) and 5 μL of NHS solution (0.1 mM in PBS 0.1 M, pH 7.2, KCl 0.1 M) for 30 min on the working electrode surface at room temperature (RT), according to a procedure reported by Gigli et al. [60]; ii) 10 μL of C-peptide Ab (10 μg/mL) was deposited on the activated electrode for 1h at 4 °C for antibody fixation. To prevent and block non-specific bindings, 5 μL of 1% w/v of BSA in PBS 0.1 M, pH 7.2, KCl 0.1 M was coated on the electrode surface for about 1 h; (iii) different human C-peptide antigen concentrations were tested to construct the calibration curve. Throughout all procedures, the electrode was kept at RT. A schematic representation of the immunosensor fabrication is shown in Scheme 1B (steps 1-4).

2.5. Real samples analysis

The human serum and urine samples were prepared from three healthy volunteers, transferred to the laboratory and centrifuged. They were filtered and stored at - 20 °C before use. Human serum and urine samples were collected 2 h after the largest meal of the day [18]. The urine samples were diluted 1:10 before analysis.

3. Results and discussion

3.1. Morphology and structural analysis of IONFs

3.1.1. SEM and TEM characterization

Fig. 1a-c displays the SEM microscopy images of IONFs modified GP-SPE at three different magnifications. It can be seen polydispersed IONFs clusters, that are formed during the polyol-based synthesis process [59]. IONFs aggregation occurred at 20 mM poly(acrylic acid) (PAA) concentrations, yielding polydisperse IONFs, with a diameter of about 20 nm. EDX spectrum reports all the emission lines expected for the IONFs composition, namely C, O, Fe. Small amounts of Si and S presence are also highlighted, probably due to impurities of the GP-SPEs (Fig. 1d).

Fig. 1e shows the TEM images of IONFs, which clearly reveal the multicore, hierarchical nanoflower morphology of the synthesized particles.

3.1.2. Raman spectroscopy characterization

To better investigate the polymorphic nature of the IONFs, micro-Raman spectra were acquired using a 514 nm excitation wavelength laser. The most representative spectra (Fig. 1f), collected at different spots on the solid-state sample, exhibit prominent bands at ~363 cm^{-1} (T_{2g}), ~509 cm^{-1} (E_g), and ~692 cm^{-1} (A_{1g}), which are characteristic of maghemite (γ-Fe_2O_3). In addition, weaker bands observed at ~222 cm^{-1} (A_{1g}) and ~290 cm^{-1} (E_g) suggest the presence of minor hematite (α-Fe_2O_3) contributions [61].

3.1.3. X-ray photoelectron spectroscopy (XPS) characterization

XPS analysis in the Fe 2p ionization region (Fig. 1g) showed a spin-orbit split doublet with components j = 3/2 and ½ separated by a ΔE_{so} ~13.5 eV and with the former feature peaked at ~710.9 eV. In order to ascertain the oxidation state of Fe, the Fe 2p spectrum was curve-fitted using the Gupta and Sen (GS) multiplets [62,63] theoretically predicted for high-spin Fe^{3+} and Fe^{2+} ions and applied by Grosvenor et al. [64,65] to magnetite and other Fe compounds. In particular, for the Fe^{3+} component a four-fold GS multiplet was used (red curves, Fig. 1g), with its first peak positioned at 710.3 eV, while a three-fold GS multiplet accounted for the Fe^{2+} component (green curves, Fig. 1g) expected for magnetit [66]. This multiplet's first peak is positioned at 708.3 eV. Additionally, two further components at 715.0 and 718.0 eV were also needed to accomplish a satisfactory curve-fitting. According to Grosvenor et al. [64], these features are respectively associated to a "surface peak" and shake-up satellite, both stemming from the Fe^{3+} component. Remarkably, the XPS Fe^{3+}/Fe^{2+} atomic ratio is 4.5, higher than the theoretical value of 2 expected for stoichiometric magnetite (Fe_3O_4), indicating an excess of Fe^{3+} species in the structure of IONFs.

The C 1s region of the IONFs sample is reported in Fig. 1h. Curve-fitting was used in order to separate the possible contributions from carbon species and ascertain their chemical state. The resulting three components are compatible with the three inequivalent C atoms of poly (acrylic acid) (PAA) [63,67] used as a capping layer in the synthesis of IONFs [59]. These components are related to the C atoms backbone (red and blue curves, at 284.8 and 286.4, respectively) and the carboxylic pendant group (green curve at 288.7 eV).

Overall, XPS results suggest that the nanoparticle surface is enriched in Fe^{3+}, consistent with the formation of Fe_2O_3 phases and in agreement with Raman analyses. On the other hand, the appearance of a Fe^{2+} component calls for the presence of an intact Fe_3O_4 core, as expected according to the adopted synthetic route [59].

3.2. Electrochemical characterization of IONFs

A preliminary surface characterization of bare and modified GP-SPEs was performed by using CV technique, which provide helpful information on the electrochemical behaviour of the graphite-SPE before and after the functionalization with IONFs. A single layer of unstructured

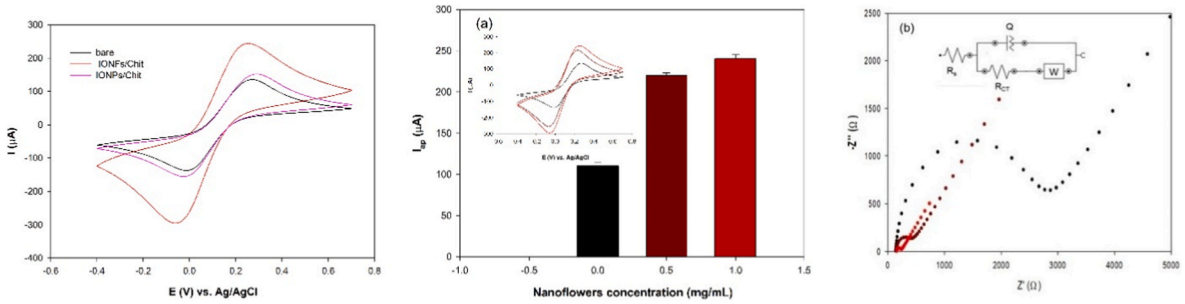


Fig. 2. (A) CVs of GP-SPE: bare (black curve), IONFs/Chit (1 mg/mL) (red curve) and IONPs/Chit (1 mg/mL) (pink curve); (B) current signal vs. IONFs concentration (a) and EIS (b) of bare (black), IONFs/Chit 0.5 mg/mL (dark red) and IONFs/Chit 1.0 mg/mL (red) GP-SPE. Data represents the mean with ± standard deviation of three replicates (n = 3). Inset (a): CVs at 100 mV/s relative to the histograms; inset (b): Randles circuit. Experimental conditions: 5 mM $[Fe(CN)_6]^{3-/4-}$ (1:1) containing 0.1 M KCl, at 100 mV/s.

chitosan (Chit) was drop-casted on the IONFs modified electrode for a better IONFs adhesion to the electrode surface. Fig. 2A shows the cyclic voltammograms obtained before (black curve) and after the modification with IONFs (IONFs/Chit, red curve) and IONPs (IONPs/Chit, pink curve), for comparison. CVs experiments were carried out in Zobell's solution, by cycling from −0.4 to 0.7 V vs Ag/AgCl, at a scan rate of 0.1 V s^{-1}. All CVs show a couple of quasi reversible redox peaks, with similar peak-to-peak separations (ΔE_p). As for the peak current intensities, the lowest peak current resulted with both bare (black curve) and IONPs modified (pink curve) electrode and the highest value with IONFs modified electrode (red curve), probably because of the improved conductivity of nanoflowers compared to nanoparticles. Fig. S1 (a, b and c) shows the CVs of bare, IONPs and IONFs modified electrode at different scan rates and the insets show the dependance of the peak current on the square root of the scan rate. It was observed that for all platforms the peak current increased linearly with the square root of the scan rate, indicating a quasi-reversible diffusion-controlled process [68]. Therefore, under the temperature of 25 ∘C, the dependence of the peak current on the square root of the scan rate was described by the following Randles-Sevcik equation:

$$I_p = 2.686 \times 10^5\, n^{3/2}\, A_{ea}\, D_0{}^{1/2} C_0\, v^{1/2}$$

where I_p is the voltametric peak current (A), n is number of electrons, A_{ea} is electroactive area (cm^2), D_0 is diffusion coefficient (7.6×10^{-6} cm^2 s^{-1} for ferricyanide), C_0 is the concentration (mol cm^{-3}) and v is the scan rate (V s^{-1}). From this equation, the electroactive area (A_e) and roughness factor (ρ) have been successively calculated and reported in Table S1. In particular, the A_{ea} has been calculated by plotting the peak current vs. square root of the scan rate ($v^{1/2}$) and inserting the slope value obtained into the following Randles-Sevcik equation [69], while the roughness factor (ρ) has been evaluated as electroactive/geometric area ratio. The A_{ea} values of the IONFs modified electrode resulted to be 3 times higher than IONPs electrodes, whereas no significant difference has been observed between IONPs and bare electrode. Table S1 shows also the heterogeneous electron transfer rate constants (k^0, cm s^{-1}) for the GP-SPE before and after the modification with IONFs and IONPs, calculated with the Lavagnini et al. method, which merges the Klingler-Kochi and Nicholson and Shain methods for irreversible and reversible systems, respectively [70]. The IONFs/Chit GP-SPE electrode showed the best performance also in terms of highest k^0 value ($k^0 = 2.01 \pm 0.11 \times 10^{-3}$ cm s^{-1}), confirming that the nano-structuration obtained with the nanoflowers promotes a faster electron transfer.

3.2.1. *Effect of IONFs concentration and loading on current response*

The effect of IONFs concentration was studied by CV, DPV and EIS in order to choose the concentration which gave the maximum current response. In particular, two different IONFs concentrations were tested (0.5 and 1.0 mg/mL). An increased peak current was observed at increasing concentrations with a maximum current at IONFs 1.0 mg/mL with both CV (Fig. 2B (a) and DPV (Fig. S2). A higher IONFs concentration did not show any significative current increase (data not shown). Therefore, 1.0 mg/mL IONFs was used for further experiments. The relative electrochemical parameters are summarized in Table S1.

EIS was also employed to study the changes due to the different NFs concentrations employed in the proposed platform. The EIS spectra were carried out in the range 0.1-10^5 Hz. Fig. 2B (b) shows the Nyquist plot for bare and modified electrodes. The semicircular at the higher frequency region and the linear part at the lower frequency region respectively stand for the electron transfer and diffusion limited process of the electrochemical reaction. A typical Randles equivalent electric circuit model (Fig. 2 B (b) inset), consisting of an active electrolyte resistance (Rs), a constant phase element (Q), a charge transfer resistance (R_{CT}), and a Warburg impedance (W), was used to fit the impedance data from the Nyquist plot. The R_{CT} values of the bare, IONFs/Chit (0.5 mg/mL) and IONFs/Chit (1.0 mg/mL) GP-SPE were estimated to be 2427 Ω, 227 Ω and 78 Ω, respectively, denoting that the electrical conductivity of the IONFs/Chit 1.0 mg/mL is much higher than that of bare and IONFs/Chit 0.5 mg/mL. Based on the R_{CT} values from EIS plots, we can estimate the standard electron transfer rate constants (k^0) for the $[Fe(CN)_6]^{3-/4-}$ system at different electrodes according to the following equation [71]:

$$k^0 = RT/(nF)^2 A C R_{CTnew}$$

where n is the electron transfer number, F the Faraday constant, A the geometric area of GP-SPE, C the concentration of the redox probe, R the ideal gas constant, and T the thermodynamic temperature.

All EIS data are summarized in Table S2.

The electron transfer rate constants of bare, IONFs/Chit 0.5 mg/mL and IONFs/Chit 1.0 mg/mL GP-SPE were estimated to be 0.37, 1.08, and 2.82×10^{-3} cm/s, respectively. The results suggest that the electron transfer rate of the latter is larger than bare and 0.5 mg/mL IONFs/Chit modified electrode. These results are in good agreement with those reported in Table S1.

The results obtained demonstrated that the proposed nanoflower morphology, after proper optimization of NFs concentration, clearly enhanced the electron transfer kinetics, showing a much larger electrochemically active surface area (A_{ea}) than the corresponding geometric area, which increases the density of redox-active sites, thus boosting the peak current in CVs (Table S1). A possible explanation is that the NFs high-curvature tips and branch edges may concentrate the electric field lines thus enhancing local electron-transfer rates, improving k^0 constants, compared to smoother nanoparticles-based films. Furthermore, well-connected, densely branched nanoflowers with good electrical continuity to the underlying electrode may reduce R_{CT} in EIS experiments (Table S2), since electrons could probably find efficient pathways through the metallic branches.

The effect of NFs loading on the electrode response was also

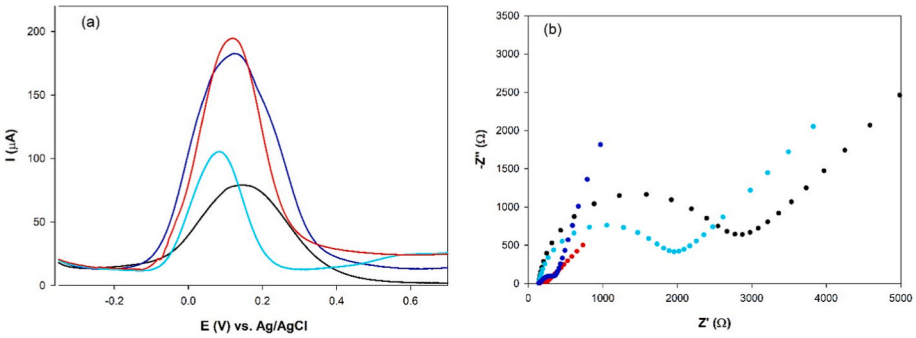


Fig. 3. (a) DPV curves and (b) EIS spectra after various modification steps: bare (black), IONFs/Chit 1.0 mg/mL(red), IONFs/Chit/EDC-NHS/Ab/BSA (blue) and IONFs/Chit/EDC-NHS/Ab/BSA/Ag (cyan) GP-SPE in 5 mM $[Fe(CN)_6]^{3-/4-}$ (1:1) containing 0.1 M KCl. The concentration of C-peptide Ab was 10 μg/mL and C-peptide Ag was 1.5 nM.

investigated by drop casting different amounts of IONFs solution (1 mg/mL in H_2O) on the electrode surface (2.5, 5, 10, 15 and 20 μL), in absence and in presence of a magnet localized under the working electrode. The histograms relative to the variations of the peak current signals vs. NFs loading are reported in Fig. S3. In absence of magnet, the biosensor response increased proportionally with the NFs loading up to 5 μL (red bars). Higher amounts result in a drastic decline of the signal response, showing the typical bell-shaped curve. In presence of the magnet during loading, a different behavior was obtained (green bars). The peak current is significantly higher than that obtained without the magnet (more than twice), even at loading values as low as 2.5 μL, thus enabling, in principle, a reduction of the NFs employed. This value remains nearly constant up to a loading of 20 μL, with a slight maximum observed at a loading of 10 μL. This experiment clearly demonstrates the importance of the use of a magnetic support during electrode modification, which helps the homogeneous distribution of the NFs on the electrode surface, thus increasing the sensitivity of the electrode and, in principle, allowing the use of a lower amount of modifier. Moreover, the magnetic attraction can exert also an indirect effect on the electron transfer, as the homogeneous, close-packed assembly reduces the possibility of electrically isolated NPs or NFs, improving the overall IONFs network across the sensing layer.

The best result is obtained with 10 μL of IONFs solution (1.0 mg/mL) drop-casted on the surface using the magnet support and therefore this was the loading used for further experiments.

3.3. Electrochemical characterization of the C-peptide immunosensor platform

The fabrication steps of C-peptide immunosensor were characterized using by differential pulse voltammetry (DPV) and electrochemical impedance spectroscopy (EIS) techniques in Zobell's solution. The changes in electrochemical performance during surface modification were recorded for each step involved in the immunosensor construction: i) GP-SPE bare; ii) IONFs/Chit; iii) IONFs/Chit/EDC-NHS/Ab/BSA; iv) IONFs/Chit/EDC-NHS/Ab/BSA/Ag. The difference in the DPV current peaks obtained after the various steps confirmed the electron surface changes during electrode modification (Fig. 3a): a large current increase is registered after the immobilization of IONFs/Chit on the surface (red curve), while a decrease is noted after the immobilization of C-peptide antibody (Ab) and BSA (blue curve), both non-conductive materials, which hinder the electron transfer. Lastly, after the adding of C-peptide antigen (Ag), a strong decrease in peak current is obtained (cyan curve), due to formation of antigen-antibody immunocomplex, thus further blocking the electron transfer between the electrode surface and the redox probe (Fig. 3a). In addition to DPV results, EIS was used to confirm the successful interface modification during immunosensor fabrication steps (Fig. 3b). A large decrease of the semicircle diameter (R_{CT}) is initially observed after the IONFs modification (red curve); then an increase of the R_{CT} values is registered after the immobilization of C-peptide antibody and BSA molecules, attesting the covalent binding of both antibody and BSA, which makes the electrode surface more insulating, causing electron transfer hindrance (blue curve). Lastly, a further significant R_{CT} increase from 86 Ω (blue curve) to 1720 Ω (cyan curve) was obtained after the binding of the C-peptide antigen, due to the hindering effect of Ab-Ag immunocomplex towards the redox probe in reaching the electrode surface.

3.4. Optimization of the C-peptide immunosensor platform

To achieve optimal detection performance, the following experimental parameters influencing the immunosensor response were systematically investigated and optimized: chitosan layer, EDC/NHS coupling conditions, BSA blocking conditions, C-peptide Ab concentration and binding time, C-peptide antigen incubation time.

The effect of the chitosan layer was indirectly investigated using CV by varying the volume of chitosan solution drop casted onto the electrode surface (Fig. S4 (a)). After the immobilization of IONFs, five different volumes of 2% chitosan solution (5, 7.5, 10, 12.5, and 15 μL) were tested.

An intermediate chitosan volume (10 μL) was selected as optimal condition, showing the highest current signal. Lower chitosan volumes (5 and 7.5 μL) were potentially insufficient to ensure complete and homogeneous coverage of the IONFs-modified electrode surface and effective entrapment of the NFs within the chitosan matrix. Further increases to 12.5 and 15 μL caused a marked decrease in peak current, indicating that an excessively thick chitosan layer hindered electron transfer and/or diffusion of the redox probe.

The optimization of the EDC/NHS coupling conditions was performed by EIS maintaining a fixed molar ratio of 5:1 and testing different concentrations (0.25/0.05, 0.5/0.1, and 1.0/0.2). An optimal EDC/NHS concentration of 0.5/0.1 was selected based on the highest specific electrochemical response obtained following C-peptide recognition (Fig. S4 (b)). Different activation times (15, 30, and 45 min) were also tested and an activation time of 30 min allowed to achieve the optimal performance of the immunosensor (data not shown).

The BSA blocking conditions were optimized by EIS at different incubation times (30, 45, 60, 75, 90 min). The results showed the ΔR_{CT} response increased up to 60 min and then reached a plateau, indicating that longer incubation times did not provide any additional blocking benefit. Therefore, a time of 60 min was selected for further experiments (Fig. S4 (c)).

The C-peptide Ab concentration was studied between 5 and 20 μg/mL by DPV technique (Fig. S4 (d)). The lowest current signal was achieved at 10 μg/mL antibody, attesting saturation of the electrode surface. The effect of C-peptide Ab binding time was successively tested recording the current obtained by DPV after 30, 45, 60, 75, and 90 min, respectively. The lowest current has been observed after 60 min Ab

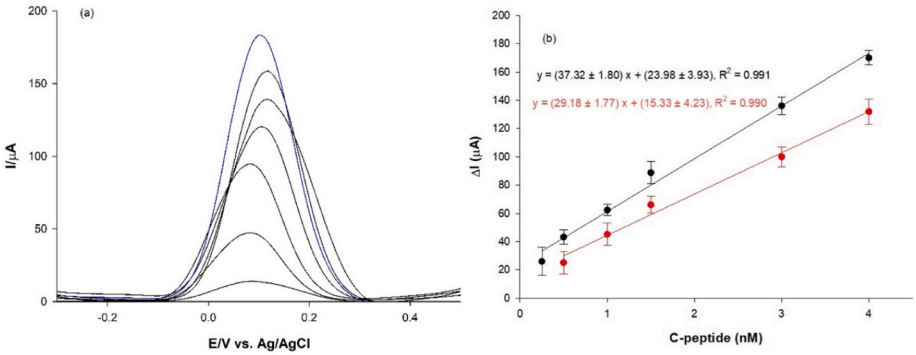


Fig. 4. (a) DPV of IONFs/Chit/EDC-NHS/Ab/BSA GP-SPE before (blue) and after the adding of different concentrations (0.25, 0.5, 1.0, 1.5, 3.0 and 4.0 nM) of C-peptide Ag (black curves) in 5 mM $[Fe(CN)_6]^{3-/4-}$ (1:1) containing 0.1 M KCl; (b) calibration curve (black), Sensit Smart calibration plot (red). Each measurement has been carried out in triplicate by using independently prepared electrodes (n = 3).

binding time. A further enhancement in time, resulted in a slight increase of the current change (Fig. S4 (e)). Thus, in further experiments, an optimum antibody concentration of 10 μg/mL was used with a binding time of 60 min. This relatively short Ab binding time is probably due to fact that the "raspberry"-like multi-core surface (IONFs) presents more accessible, hydroxyl-rich area than a smooth sphere (IONPs) of the same overall hydrodynamic size, giving more anchoring points per captured entity, thus probably allowing a higher antibody immobilization efficiency.

Finally, the C-peptide antigen incubation time was investigated at 30, 45, 60, and 75 min. The optimization the antigen incubation time is essential to avoid excessive antigen binding and to maintain a balance for efficient electron transfer. The current DPV change initially decreased with increasing antigen incubation time up to 60 min, as shown in Fig. S4 (f). A longer Ag incubation time is prone to increasing the current change, as an excessive antigen binding might block the electron transfer. The antigen saturation was reached for the optimized antibody concentration after 60 min incubation time, and therefore this was used for further experiments.

3.5. Analytical performance of C-peptide immunosensor

Under optimal conditions, the analytical performance of the proposed immunosensor was evaluated toward different concentrations of human C-peptide (0.25, 0.5, 1.0, 1.5, 3.0 and 4.0 nM) by DPV technique, which is known to have higher consistency compared to CV, by using three independently prepared electrodes. The results, shown in Fig. 4a, are calculated from the difference between the signal peak before (blue curve) and after the addition of C-peptide (black curves). The peak current decreases with increasing C-peptide concentration and the calibration curve obtained (Fig. 4b) shows a high sensitivity (339 μA nM^{-1} cm^{-2}), a linear relationship in the range 0.25-4 nM and a low LOD of 70 pM, estimated as $3S_b/m$ formula, where S_b is the standard deviation of the blank, and m is the slope of the calibration curve. These three values together make the proposed immunosensor suitable to perform the analysis in the clinically relevant range.

Further, the immunosensor was used with a portable potentiostat directly connected to a smartphone for POC signal reading showing a slightly shorter dynamic linear range between 0.5 and 4 nM, a LOD of 150 pM and a slightly lower sensitivity of 265 μA nM^{-1} cm^{-2}, values within the clinically relevant range for C-peptide detection.

3.6. Reproducibility, stability and selectivity of C-peptide immunosensor

The inter-electrode reproducibility of our immunosensor was tested by calculating the relative standard deviation (RSD%) value of five different platforms at 1.5 nM C-peptide. An RSD of about 5% has been obtained, confirming a reasonably reproducibility of our system, as shown in Fig. S5 (a).

The stability of the C-peptide platform was also investigated by storing the electrode, after modification with IONFs and C-peptide antibody, dry at 4 °C for 4 weeks, and monitoring the current signal by DPV experiments at regular intervals of 7 days. The signal remained almost stable up to 4 weeks (RSD% of about 1.7%), retaining 95% of its initial current signal (Fig. S5 (b)).

The selectivity of the platform was studied by testing the ability of the biosensor to detect C-peptide in presence of the following interferents: glucose (GLU, 5 mM), uric acid (UA, 5 mM), ascorbic acid (AA, 5 mM), glutathione (GSH, 5 mM), creatinine (CREA 5 mM), albumin (ALB 5 mM), insulin (Ins, 0.5 nM) and proinsulin (Pro Ins 0.5 nM). DPV signal decreases were registered after 60 min incubation period of each compound tested, compared to 0.5 nM C-peptide, on the IONFs/Chit/C-peptide Ab/BSA/GP-SPE platform, as shown in Fig. S5 (c). These results show the high selectivity of the proposed biosensor, as no significant signal has been registered with each interferent tested, although GLU, UA, AA, GSH, CREA and ALB were added at a concentration $1x10^7$-fold than C-peptide. As for Ins and Pro Ins, they have been tested at the same C-peptide concentration, even though their concentration in serum is much lower, about 0.014–0.140 nM and 0.005–0.023 nM in fasting healthy individuals for insulin and proinsulin, respectively [7,10].

A plausible explanation for the absence of significant interference from insulin is that, despite insulin and C-peptide derive from the common precursor proinsulin, they share no primary sequence homology or overlapping epitopes, and consequently the antibody selected against C-peptide exhibits negligible cross-reactivity toward insulin. In the case of proinsulin, which does contain the C-peptide sequence, it is possible, in principle, a residual cross-reactivity. However, the results obtained confirm the absence of significant cross-reactivity, probably because the commercial antibody against C-peptide used in this study contains carefully chosen epitopes, generated upon proteolytic cleavage, that allow to recognise free C-peptide while not binding intact proinsulin.

Four independently manufactured batches of the biosensor were used to assess the batch-to-batch repeatability. Three sensors were chosen at random from each batch and tested under the same experimental settings. The mean current response was quite constant across the four batches (88.02, 88.60, 88.70, and 88.28 μA for batches 1-4, respectively), as shown in Fig. S5 d. Excellent fabrication reproducibility and great manufacturing consistency were demonstrated by the RSD values, which varied from 0.87% to 1.29%. These findings show that the suggested fabrication process offers consistent sensor performance with low batch-to-batch variability.

Table 1
Comparison of C-peptide detection with the proposed immunosensor in human serum and urine and a conventional HPLC-UV method.

Human Sample	Human serum and urine C-peptide concentrations (ng/mL)					
	Immunosensor[a] *(serum)*	*HPLC-UV*[a] *(serum)*	*Relative Error (%)*	*Immunosensor*[a] *(urine)*	*HPLC-UV*[a] *(urine)*	*Relative Error (%)*
patient 1	0.82 ± 0.07[b]	0.90 ± 0.03	8.8	10.11 ± 0.68	10.85 ± 0.54	6.8
patient 2	1.10 ± 0.08	1.17 ± 0.05	5.9	15.44 ± 0.85	16.90 ± 0.65	8.6
patient 3	3.18 ± 0.06	3.30 ± 0.03	3.6	31.22 ± 0.90	32.40 ± 0.71	3.6

[a] Every test for each patient was repeated 3 times (N = 3). The value reported in Table 1 is the average value.
[b] RSD based on three replicate analyses.

3.7. Application of the immunosensor for the human C-peptide detection in real serum/urine samples

The proposed immunosensor was tested in serum and urine of 3 fasting healthy volunteers, in order to demonstrate the capability of the C-peptide immunosensor to measure C-peptide levels in real clinical samples. The collected samples were also analyzed by HPLC-UV, used as reference method, and the results are reported in Table 1. The excellent agreement obtained (% difference $\leq$ 9%), confirms the good performance of the developed immunosensor.

It is possible to note that the C-peptide levels in urine are more than 10 times higher than in serum, as C-peptide is not degraded by proteolytic enzymes. Patient 1 and 2 show C-peptide levels in the typical range for healthy adults, whereas patient 3 show a higher level (>3.0 ng/mL), which may indicate insulin resistance condition, which can be considered a prediabetic stage with an increased risk of progression towards type 2 diabetes [18,20].

The study conducted on three subjects represents a preliminary pilot study and will be extended to a larger cohort of volunteers, including both healthy and diabetic participants.

3.8. Comparison of the immunosensor performance with other biosensors for C-peptide detection

The analytical performance of the proposed biosensor was compared to other works recently published in literature (Table S3)[48–54,72]. As can be seen, most of them are based on fluorescence or electrochemiluminescence (ECL) detection methods. As for optical methods, the sensitivities shown by fluorescence- [69] and SERS-based [49] methods resulted definitely higher, if compared to electrochemical methods. However, they suffer from the high instrumental complexity and costs, and limited portability that limits POC applications. As far as the electrochemical detection, the only work has been published by Jalalvand and Pinto [54] about a molecularly imprinted (MIP) biosensor for the detection of insulin, proinsulin and C-peptide, with a very low LOD but a short linear range (up to 88 pM), which does meet clinical needs. Electrochemical biosensors based on MIPs are reported to achieve picomolar or sub-picomolar concentrations. However, they suffer from lack of reproducibility between batches. Moreover, the fabrication process is complex, time consuming and economically unfeasible [73], as the biosensor was developed by modifying a thick-film boron-doped diamond electrode with a multi-walled carbon nanotubes (MWCNTs-C60) graphite ionic liquid nanocomposite [54], utilizing triple-template molecularly imprinted polymers. To begin with, the starting material of the electrode, a boron-doped diamond electrode, is much more expensive compared to graphite used in our sensor. Furthermore, the fabrication process involves more steps, first adding MWCNTs and then MIPs, which makes the procedure longer and more complex. Here, the proposed biosensor allows a cheap, fast, disposable and more reproducible system, easily useable at the POC, with a wider linear range, across the clinically relevant range for C-peptide detection, although with a slightly higher LOD.

4. Conclusions

A disposable label-free electrochemical immunosensor based on a graphite SPE functionalized with magnetic IONFs was demonstrated to successfully work for POC detection of C-peptide in human serum and urine. C-peptide detection holds considerable promise, not being subjected to exogeneous insulin interference, in refining diabetes diagnosis and treatment. In particular, it could be used for a routine screening in at-risk patients, as well as prediabetic diagnosed T1D and T2D populations, to enable comprehensive assessment of diabetes category and stage, thus facilitating the application of precision medicine to diabetes management and care.

The magnet-assisted modification of the graphite electrode surface with the IONFs resulted in a superior enhancement in the registered CV current compared to the signal obtained with IONPs modification without the magnet, and with IONPs. The magnet-assisted assembly resulted to be a useful strategy for both improving physical homogeneity of the sensing layer and indirectly enhancing electron communication. After the optimization of all analytical parameters, the immunosensor displayed a high level of selectivity and sensitivity towards C-peptide.

The potential of the proposed biosensor is mainly attributed to the preparation simplicity, reproducibility, low cost and portability, which gives this type of biosensor an edge over traditional methods, in particular for the significant reduction in costs and time (from hours to a few minutes).

These promising features are thus encouraging to introduce the proposed immunosensor as a reliable method for C-peptide POC determination in human serum and urine samples.

CRediT authorship contribution statement

Cristina Tortolini: Methodology, Investigation, Data curation. **Francesco Dotta:** Funding acquisition. **Andrea Giacomo Marrani:** Methodology. **Francesco Amato:** Validation, Software. **Andrea Lenzi:** Funding acquisition. **Liudmyla Storozhuk:** Methodology. **Nguyen Thi Kim Thanh:** Validation, Supervision. **Riccarda Antiochia:** Writing – review & editing, Supervision, Project administration.

Declaration of competing interest

The authors declare that they have no known competing financial interests or personal relationships that could have appeared to influence the work reported in this paper.

Acknowledgments

The work has been supported by the Project PNC 0000001 D3 4Health – CUP B53C22006120001, The National Plan for Complementary Investments to the NRRP, Funded by the European Union – NextGenerationEU.

Appendix A. Supplementary data

Supplementary data to this article can be found online at https://doi.

org/10.1016/j.talanta.2026.130865.

Data availability

Data will be made available on request.

References

[1] G.L.C. Yosten, C. Maric-Bilkan, P. Luppi, J. Wharen, Physiological effects and therapeutic potential of proinsulin C-peptide, am, J. Endocrinol Metab 307 (2014) E955, https://doi.org/10.1152/ajpendo.00130.2014.

[2] S.K. Venugopal, M.L. Mowery, I. Jialal, Biochemistry, C Peptide. Statpearls. Treasure Island (FL): Statpearls Publishing Copyright © 2024, StatPearls Publishing LLC, 2024.

[3] S. Lenzen, The pancreatic beta cell: an intricate relation between anatomical structure, the signalling mechanism of glucose-induced insulin secretion, the low antioxidative defence, the high vulnerability and sensitivity to diabetic stress, ChemTexts 7 (2021) 13, https://doi.org/10.1007/s40828-021-00140-3.

[4] D. Brandenburg, History and diagnostic significance of C-peptide, Exp. Diabetes Res. 2008 (2008) 576862, https://doi.org/10.1155/2008/576862.

[5] Y. An, Insulin secretory granule biogenesis and VPS41. https://hdl.handle.net/2123/31484, 2023.

[6] J.B. Field, Extraction of insulin by liver, Annu. Rev. Med. 24 (1973) 309, https://doi.org/10.1146/annurev.me.24.020173.001521.

[7] A.I. Katz, A.H. Rubenstein, Metabolism of pro-insulin, insulin and C-peptide in the rat, J. Clin. Investig. 52 (1973) 1113, https://doi.org/10.1172/jci107277.

[8] M. Liu, M.A. Weiss, A. Arunagiri, J. Yong, N. Rege, J. Sun, L. Haataja, R. J. Kaufman, P. Arvan, Biosynthesis, structure, and folding of the insulin precursor protein, Diabetes Obes. Metabol. 20 (2018) 28, https://doi.org/10.1111/dom.13378.

[9] S.Y. Park, J.F. Gautier, S. Chon, Assessment of insulin secretion and insulin resistance in human, Diabetes Metab. J 45 (2021) 641, https://doi.org/10.4093/dmj.2021.0220.

[10] W.C. Duckworth, R.G. Bennett, F.G. Hamel, Insulin degradation: progress and potential, Endocr. Rev. 19 (1998) 608, https://doi.org/10.1210/edrv.19.5.0349.

[11] D.S. Abdulateef, J.M. Salih, Detection of C-Peptide in scalp hair of healthy adults, diabetes, Metab. Syndr. Obes. 13 (2020) 227, https://doi.org/10.2147/dmso.s240785.

[12] A.G. Jones, A.T. Hattersley, The clinical utility of C-peptide measurement in the care of patients with diabetes, Diabet. Med. 30 (2013) 803, https://doi.org/10.1111/dme.12159.

[13] J. Chen, Y. Huang, C. Liu, J. Chi, Y. Wang, L. Xu, The role of C-peptide in diabetes and its complications: an updated review, Front. Endocrinol. 14 (2023) 1256093, https://doi.org/10.3389/fendo.2023.1256093.

[14] D. Brandenburg, History and diagnostic significance of C-peptide, Exp, Diabetes Res. 2008 (2008) 576862, https://doi.org/10.1155/2008/576862.

[15] Bhuvaneswari Ponnusamy, Ponnulakshmi Rajagopal, Raktim Mukherjee, Swetha Panneerselvam, Selvaraj Jayaraman, Diabetes management: from“painful” Pricks to “Pain-Free” bliss, in: R. Noor (Ed.), Advances in Diabetes Research and Management, Springer Nature Singapore, Singapore, 2023, pp. 195–223, https://doi.org/10.1007/978-981-19-0027-3_9.

[16] A.A. Khazaal, M.K. Yousif, A.J. Hendi, D. Atwan, Serum C-peptide levels as a predictor of beta-cell function in children with type 1 diabetes, RJDNMD 30 (2023) 375. https://www.rjdnmd.org/index.php/RJDNMD/article/view/1442.

[17] S. Iqbal, A.A. Jayyab, A.M. Alrashdi, S. Reverté-Villarroya, The predictive ability of C-Peptide in distinguishing type 1 diabetes from type 2 diabetes: a systematic review and meta-analysis, Endocr. Pract. 29 (2023) 379, https://doi.org/10.1016/j.eprac.2023.01.004.

[18] E.S. Vinay, B. Laxmi Narsimha Rao, N. Saf, D. Gautam, C-peptide in precision diabetes care and beyond: a comprehensive review, Clin. Med. Insights Endocrinol. Diabetes 19 (2026) 1, https://doi.org/10.1177/11795514251397811. /nost.

[19] E. Maddaloni, G.B. Bolli, B.M. Frier, R.R. Little, R.D. Leslie, R. Buzzetti, C-peptide determination in the diagnosis of type of diabetes and its management: a clinical perspective, Diabetes Obes. Metabol. 24 (2022) 1912, https://doi.org/10.1111/dom.14785.

[20] G.L.C. Yosten, C. Maric-Bilkan, P. Luppi, J. Wahren, Physiological effects and therapeutic potential of pro-insulin C-peptide, Am. J. Physio. Endocrinol. Metab. 307 (2014) E955, https://doi.org/10.1152/ajpendo.00130.2014.

[21] E. Leighton, C. Sainsbury, G.C. Jones, A practical review of C-peptide testing in diabetes, Diabetes Ther 8 (2017) 475, https://doi.org/10.1007/s13300-017-0265-4.

[22] A.G. Jones, A.T. Hattersley, The clinical utility of C-peptide measurement in the care of patients with diabetes, Diabet. Med. 30 (2013) 803, https://doi.org/10.1111/dme.12159.

[23] T. Iwao, K. Sakai, M. Sata, Postprandial serum C-peptide is a useful parameter in the prediction of successful switching to liraglutide monotherapy from complex insulin therapy in Japanese patients with type 2 diabetes, J. Diabetes Complications 27 (2013) 87, https://doi.org/10.1016/j.jdiacomp.2012.07.001.

[24] B.Y. Kim, C.H. Jung, J.O. Mok, S.K. Kang, C.H. Kim, Association between serum C-peptide levels and chronic microvascular complications in Korean type 2 diabetic patients, Acta Diabetol. 49 (2012) 9, https://doi.org/10.1007/s00592-010-0249-6.

[25] J. Wahren, C-peptide and the pathophysiology of microvascular complications of diabetes, J. Intern. Med. 281 (2017) 3, https://doi.org/10.1111/joim.12541.

[26] M. Cardellini, A. Farcomeni, M. Ballanti, M. Morelli, F. Davato, I. Cardolini, G. Grappasonni, S. Rizza, V. Guglielmi, O. Porzio, C. Pecchioli, R. Menghini, A. Ippoliti, M. Federici, C-peptide: a predictor of cardiovascular mortality in subjects with established atherosclerotic disease, diabetes Vasc, Dis. Res. 14 (2017) 395, https://doi.org/10.1177/1479164117710446.

[27] D. Vasic, D. Walcher, C-peptide: a new mediator of atherosclerosis in diabetes, Mediat. Inflamm. 2012 (2012) 1, https://doi.org/10.1155/2012/858692.

[28] J.O. Chung, D.H. Cho, D.J. Chung, M.Y. Chung, Relationship between serum C-peptide level and diabetic retinopathy according to estimated glomerular filtration rate in patients with type 2 diabetes, J. Diabetes Complications 29 (2015) 350, https://doi.org/10.1016/j.jdiacomp.2014.12.013.

[29] E. Leighton, C. Sainsbury, G.C. Jones, A practical review of C-peptide testing in diabetes, Diabetes Ther 8 (2017) 475, https://doi.org/10.1007/s13300-017-0265-4.

[30] A. Maheshwari, Insights on C-peptide in diabetes, J. Nutr. Metab. Health Sci. 6 (2023) 63, https://doi.org/10.18231/j.ijnmhs.2023.009.

[31] E. Latres, C.J. Greenbaum, M.L. Oyaski, C.M. Dayan, H.M. Colhoun, J.M. Lachin, J. S. Skyler, M.R. Rickels, S.T. Ahmed, S. Dutta, K.C. Herold, M. Marinac, Evidence for C-peptide as a validated surrogate to predict clinical benefits in trials of disease-modifying therapies for Type 1 diabetes, Diabetes 73 (2024) 823, https://doi.org/10.2337/dbi23-0012.

[32] M.L. Graham, S.C. Gresch, S.K. Hardy, L.A. Mutch, J.L. Janecek, R.L. Hegstad-Davies, Evaluation of commercial ELISA and RIA for measuring porcine C-peptide: implications for research, Xenotransplantation 22 (2015) 62, https://doi.org/10.1111/xen.12143.

[33] R.R. Rasmi, V.B. Kadwad, J. Sarnaik, K.B. Shenoy, H.M. Somashekarappa, Development of radioimmunoassay for estimation of C-peptide in human serum, J. Radioanal. Nucl. Chem. 327 (2021) 923, https://doi.org/10.1007/s10967-020-07536-4.

[34] N. Bano, S. Ahmed, C-peptide: performance evaluation electrochemiluminescence immunoassays, Clin. Chim. Acta 558 (2024) 118462, https://doi.org/10.1016/j.cca.2024.118462.

[35] N. Foulon, E. Goonatilleke, M.J. MacCoss, M.A. Emrick, A.N. Hoofnagle, Multiplexed quantification of insulin and C-peptide by LC-MS/MS without the use of antibodies, JMSACL 25 (2022) 19, https://doi.org/10.1016/j.jmsacl.2022.06.003.

[36] R.E. Foreman, C.L. Meek, G.P. Roberts, A.L. George, F. Reimann, F.M. Gribble, R. G. Kay, LC-MS/MS based detection of circulating proinsulin derived peptides in patients with altered pancreatic beta cell function, J. Chromatogr. B 1211 (2022) 123482, https://doi.org/10.1016/j.jchromb.2022.123482.

[37] K. Kabytaev, E. Maddaloni, M.L. Ferm, M.J. Redondo, R. Buzzetti, P. Pozzilli, C-peptide as an important biomarker in diabetes management: the need for standardization of its measurement, Diabetes Obes. Metabol. 28 (2026) 2503, https://doi.org/10.1111/dom.70447.

[38] T. Phumlani, S. Poslet Morgan, N.T. Zikhona, Biosensors: design, development and applications, in: A. Sadia, M.S. Akhtar, S. Hyung-Shik (Eds.), Nanopores, IntechOpen, 2021, https://doi.org/10.5772/intechopen.97576.

[39] D. Bhatia, S. Paul, T. Acharjee, S.S. Ramachairy, Biosensors and their widespread impact on human health, Sens. Int. 5 (2024) 100257, https://doi.org/10.1016/j.sintl.2023.100257.

[40] S. Yadav, A. Saini, R. Devi, S. Lata, Transducers in biosensors, in: P. Kumar, S. K. Dash, S. Ray (Eds.), Biomaterials-Based Sensors, Springer Nature Singapore, Singapore, 2023, pp. 101–125, https://doi.org/10.1007/978-981-19-8501-0_4.

[41] A. Haleem, M. Javaid, R.P. Singh, R. Suman, S. Rab, Biosensors applications in medical field: a brief review, Sens. Int. 2 (2021) 100100, https://doi.org/10.1016/j.sintl.2021.100100.

[42] C. Lino, S. Barrias, R. Chaves, F. Adega, P. Martins-Lopes, J.R. Fernandes, Biosensors as diagnostic tools in clinical applications, Biochimica et Biophysica Acta (BBA) - reviews on, Cancer 1877 (2022) 188726, https://doi.org/10.1016/j.bbcan.2022.188726.

[43] S. Esmaeelzadeh, N. Akbarzadeh-T, Bimetallic nanoparticle of yttrium-copper metal-organic framework (Y-Cu-MOF) as a novel modifier for determination of ascorbic acid, Adv. J. Nanochem. Med. 1 (2025) 220, https://doi.org/10.48309/ajnm.2025.551291.1019.

[44] H. Sarhadi, S. Moshrefi, B. Rezaei Zadeh, Application of a modified graphite screen-printed electrode for sensitive detection of vitamin C, Adv. J. Nanochem. Med. 1 (2025) 233, https://doi.org/10.48309/ajnm.2025.537234.1014.

[45] I.A. Jihad, T.J. Jassim, Z.N. Mageed, Efficient electrochemical determination of dopamine in the presence of uric acid in real samples using tungsten disulfide nanostructure modified electrode, ADMET and DMPK 13 (2025), https://doi.org/10.5599/admet.2968.

[46] P. Mohammadzadeh Jahani, M. Jafari, Norepinephrine detection using modified carbon paste electrode, Journal of Environmental and Bioanalytical Electrochemistry 2 (2026) 22, https://doi.org/10.48309/jebe.2026.531889.1027.

[47] Zahra Jamalizadeh Bahaabadi, Prashant Kesharwani, Amirhossein Sahebkar, Detecting C-peptide using biosensors for diagnosis and monitoring of disease, Microchem. J. 207 (2024) 111922, https://doi.org/10.1016/j.microc.2024.111922.

[48] E. Heyduk, M.M. Moxley, A. Salvatori, J.A. Corbet, T. Heyduk, Homogeneous insulin and C-peptide sensors for rapid assessment of insulin and C-peptide secretion by the islets, Diabetes 59 (2010) 2360, https://doi.org/10.2337/db10-0088.

[49] T. Zhang, H. Wu, C. Qiu, M. Wang, H. Wang, S. Zhu, Y. Xu, Q. Huang, S. Li, Ultrasensitive hierarchical AuNRs@SiO2@Ag SERS probes for enrichment and detection of insulin and C-Peptide in serum, Int. J. Nanomed. 19 (2024) 6281, https://doi.org/10.2147/ijn.s462601.

[50] X. Liu, C. Fang, J. Yan, H. Li, Y. Tu, A sensitive electrochemiluminescent biosensor based on AuNP-functionalized ITO for a label-free immunoassay of C-peptide, Bioelectrochemistry 123 (2018) 211, https://doi.org/10.1016/j.bioelechem.2018.05.010.
[51] H. Wang, L. Peng, Y. Chai, R. Yuan, High-sensitive electrochemiluminescence C-peptide biosensor via the double quenching of dopamine to the novel Ru(II)-Organic complex with dual intramolecular self-catalysis, Anal. Chem. 89 (2017) 11076, https://doi.org/10.1021/acs.analchem.7b03125.
[52] P.V. Rao, E. Bean, D. Nair-Schaef, S. Chen, S.C. Kazmierczak, C.T. Roberts, S. R. Nagalla, Rapid point-of-care test for determination of C-Peptide levels, J. Diabetes Sci. Technol. 16 (2022) 976, https://doi.org/10.1177/1932296821995557.
[53] S. Chen, Z. Guo, B. Lu, M. Sun, S. Wang, S. Li, Y. Jiang, Q. Wei, D. Wang, X. Jiang, A wearable device for continuous immunoassay-based monitoring of C-peptide in interstitial fluid, Sci. Adv. 11 (2025) eadw2182, https://doi.org/10.1126/sciadv.adw2182.
[54] A.R. Jalalvand, L. Pinto, A novel triple templates molecularly imprinted biosensor assisted by second-order calibration methods based on generation of second-order hydrodynamic linear sweep voltammetric data for simultaneous biosensing of insulin, proinsulin and C-peptide: application to comparing PARAFAC2 and PARASIAS chemom, Intel. Lab. Syst. 233 (2023) 10476, https://doi.org/10.1016/j.chemolab.2022.104746.
[55] S.J. Lee, H. Jang, D.N. Lee, Recent advances in nanoflowers: compositional and structural diversification for potential applications, Nanoscale Adv. 5 (2023) 5165, https://doi.org/10.1039/D3NA00163F.
[56] M. Yıldırım, M.T. Aminzai, E. Yabalak, Nanoflowers: a multifunctional nanomaterial revolutionizing medicine, environmental protection, and sustainable agriculture, Inorg. Chem Comm. 177 (2025) 114311, https://doi.org/10.1016/j.inoche.2025.114311.
[57] P.R.S. Baabu, H.K. Kumar, M.B. Gumpu, K.J. Babu, A.J. Kulandaisamy, J.B. B. Rayappan, Iron oxide nanoparticles: a review on the province of its compounds, properties and biological applications, Materials 16 (2023) 59, https://doi.org/10.3390/ma16010059.
[58] A.S. Agnihotri, V.G. Anitha, M. Nidhin, Transition metal oxides in electrochemical and bio sensing: a state-of-art review, Appl. Surf. Sci. Adv. 4 (2021) 100072, https://doi.org/10.1016/j.apsadv.2021.100072.
[59] L. Storozhuk, M.O. Besenhard, S. Mourdikoudis, A.P. LaGrow, M.R. Lee, L. Duc Tung, A. Gavriilidis, N.T.K. Thanh, Stable iron oxide nanoflowers with exceptional magnetic heating efficiency: simple and fast polyol synthesis, ACS Appl. Mater. Interfaces 13 (2021) 45870, https://doi.org/10.1021/acsami.1c12323.
[60] V. Gigli, C. Tortolini, E. Capecchi, A. Angeloni, A. Lenzi, R. Antiochia, Novel amperometric biosensor based on tyrosinase/chitosan nanoparticles for sensitive and interference-free detection of total catecholamine, Biosensors 12 (2022) 519, https://doi.org/10.3390/bios12070519.
[61] A.M. Jubb, H.C. Allen, Vibrational spectroscopic characterization of hematite, maghemite, and magnetite thin films produced by vapor, deposition, Appl. Mater. Interfaces 2 (2010) 2804, https://doi.org/10.1021/am1004943.
[62] R.P. Gupta, S.K. Sen, Calculation of multiplet structure of core *p*-vacancy levels, Phys. Rev. B 10 (1974) 71, https://doi.org/10.1103/PhysRevB.10.71.
[63] R.P. Gupta, S.K. Sen, Calculation of multiplet structure of core *p* -vacancy levels. II, Phys. Rev. B 12 (1975) 15, https://doi.org/10.1103/PhysRevB.12.15.
[64] A.P. Grosvenor, B.A. Kobe, M.C. Biesinger, N.S. McIntyre, Investigation of multiplet splitting of Fe 2p XPS spectra and bonding in iron compounds, Surf. Interface Anal. 36 (2004) 1564, https://doi.org/10.1002/sia.1984.
[65] M.C. Biesinger, B.P. Payne, A.P. Grosvenor, L.W.M. Lau, A.R. Gerson, R.StC. Smart, Resolving surface chemical states in XPS analysis of first row transition metals, oxides and hydroxides: cr, Mn, Fe, Co and Ni, Appl. Surf. Sci. 257 (2011) 2717, https://doi.org/10.1016/j.apsusc.2010.10.051.
[66] F. Hajareh Haghighi, R. Binaymotlagh, L. Chronopoulou, S. Cerra, A.G. Marrani, F. Amato, C. Palocci, I. Fratoddi, Self-assembling peptide-based magnetogels for the removal of heavy metals from water, Gels 9 (2023) 621, https://doi.org/10.3390/gels9080621.
[67] H. Hantsche, High resolution XPS of organic polymers, the scienta ESCA300 database. By G. Beamson, D. Briggs, wiley, Chichester, 1992, pp. 295, Adv. Mater 5 (1993) 778, https://doi.org/10.1002/adma.19930051035.
[68] Z. Masood, H. Muhammad, I.A. Tahiri, Comparison of different electrochemical methodologies for electrode reactions: a case study of paracetamol, Electrochem 5 (2024) 57, https://doi.org/10.3390/electrochem5010004.
[69] K.B. Oldham, Analytical expressions for the reversible randles-sevcik function, J. Electroanal. Chem. Interfacial Electrochem. 105 (1979) 373, https://doi.org/10.1016/S0022-0728(79)80132-1.
[70] I. Lavagnini, R. Antiochia, F. Magno, A calibration-based method for the evaluation of the detection limit of an electrochemical biosensor, Electroanalysis 19 (2007) 1227, https://doi.org/10.1002/elan.200703847.
[71] N.N.A. Kamal, N.S. Anuar, R. Noordin, A. Rahumatullah H.H. Hamzah, Electrodeposited gold nanoparticle (AuNP)-Film as a nanoplatform for a label-free electrochemical strongyloidiasis immunosensor, J. Electrochem. Soc. 169 (2022) 106514, https://doi.org/10.1149/1945-7111/ac9434.
[72] B. Yu, Y. Cui, X. Mao, Z. Li, Z. Li, G. Shi, A time-resolved fluorescence lateral flow immunochromatographic assay based on oriented immobilized antibodies for the ultrasensitive detection of C-peptides in human serum, Anal. Chim. Acta 1208 (2022) 339833, https://doi.org/10.1016/j.aca.2022.339833.
[73] A.J. Kadhem, G.J. Gentile, M.M. Fidalgo de Cortalezzi, Molecularly imprinted polymers (MIPs) in sensors for environmental and biomedical applications: a review, Molecules 26 (2021) 6233, https://doi.org/10.3390/molecules26206233.